Vol. 44, No. 4 (2022) 24-38, DOI: 10.24874/ti.1025.12.20.04

Tribology in Industry

www.tribology.rs

RESEARCH

Estimation of Wear Performance of Al-based Composite Reinforced with Al_2O_3 and MoS_2 Using Taguchi Approach

Hari Kiran Vuddagiri[a,*], Hota Ravisankar [b]

[a]*Department of Mechanical Engineering, Avanthi Institute of Engineering and Technology, Narsipatnam, Andhra Pradesh, India,*
[b]*Department of Mechanical Engineering, GITAM University, Visakhapatnam, Andhra Pradesh, India.*

Keywords:

AMCs
Wear rate
Coefficient of friction
Alumina (Al_2O_3)
Molybdenum disulfide (MoS_2)

* Corresponding author:

Hari Kiran Vuddagiri
E-mail: harikiran3285@gmail.com

Received: 21 December 2020
Revised: 7 February 2021
Accepted: 13 April 2021

A B S T R A C T

The present study is focused on the tribological performance of Molybdenum disulfide (MoS_2), and Alumina (Al_2O_3) used as reinforcement in Al-Si-Mg alloy. By adapting the stir casting route, aluminum matrix composites (AMCs) are manufactured. The process variables such as weight percent of reinforcement i.e., Al_2O_3 (4, 8, 12 and 16 wt. percent), and MoS_2 (2 and 4 wt. percent), sliding velocity (1 m/s, 1.5 m/s, and 2 m/s), and load (10, 20 and 30 N), on tribological responses are wear rate and coefficient of friction. The experiments are intended to use the Taguchi Orthogonal array (L27). Mechanical properties such as hardness and tensile strength have been evaluated and hybrid metal matrix composites (HMC) have shown significant improvement. Analysis of Variance (ANOVA) revealed wear rate and coefficient of friction decreased with an increase in sliding speed and increased with the applied load. The worn-out, fractured composite surfaces are examined by a scanning electron microscope (SEM). A predominant wear mechanism is observed at low load has a combination of adhesive and abrasive wear, accompanied by high load as adhesive wear. The hybrid composites exhibited improved wear resistance and low friction coefficient as compared to the base alloy.

1. INTRODUCTION

Of the ever-increasing demands as well as intricacy of new technologies, technologists are actively finding highly sophisticated materials, light-weighted and high-performance components for hottest time-use activities like the automotive industry. Those attributes have become too difficult to achieve in such conventional materials. Composite materials are receiving much attention for enhancing the properties of pure metal nowadays. Aluminum is widely used in various automotive eras, as opposed to several other widely employed

materials owing to, corrosion resistance, high strength to weight ratio, specific heat, low melting point etc. Aluminium applications includes the variety of sectors for their particular distinct advantages, including household appliances, transportation, manufacturing, and trade [1–3].

Mostly in context of wear resistance, having lubrication is crucial to minimize wear. It is difficult to provide lubricant across interfaces of components to minimize wear. Self-lubricated components are representatives of a lubricant that could be discharged instantly during the wear process. Nowadays, graphite and molybdenum disulphide are the most widely used solid lubricant ingredients [4–6].

Generally, the effect of graphite depends on the formation of film thickness which in turn depends on many factors that result in graphite extrusion. Hard graphite offers good lubrication at high humidity, high temperature durability, and corrosion resistance against fretting, low friction coefficient under extremely high loads [7]. Molybdenum disulfide is an excellent adhesion property that reduces friction at higher loads, high load carrying capacity, stick slip prevention, fretting corrosion protection etc. The size of the lubricant particles also affects the friction coefficient. Large size lubricant particulate matter shows a better result at low speed in rough surfaces and a fine lubricant particle performs best at high velocity on smooth surfaces [8,9].

The surface of MoS_2 is seen to be lamellae structure and sliding direction is orient parallel. Therefore, MoS_2 is help to slide easily, which leading to low friction of components under various pressures. Such lubricants help in maintaining a low coefficient of friction in between areas of contact due to the weak bonding between materials in a superficial context. These layers will slide with minimal force applied proportional to each other, thereby gaining themselves low drag properties. Of this purpose, graphite and MoS_2 have used in industrial applications [10].

The effects of tribological and mechanical behavior of Al-Si10Mg Al-Si10Mg/MoS_2 composites were studied by Vinoth et al [9]. They found that the hardness, elongation and tensile strength of composites are decreased with an addition of MoS2 particles. The composite with 2 wt.% MoS_2 and 4 wt.% MoS_2 show a decrease trend in the wear rate by 55% and 65%, respectively, compared with the base alloy.

Upadhyay and Kumar [11] prepared ternary composites of epoxy-graphene-MoS_2 and established composite properties such as physical - chemical, thermal, and tribological behaviours. They revealed that the ternary epoxy-graphene-MoS_2 composite, compared with the binary epoxy-graphene and epoxy-MoS_2 composites, helped reduce friction and wear rate. The ternary composites showed the friction coefficient in the range of 0.0023–0.0048 and the wear rate was found between 1.22 $x10^{-7}$ – 1.44 x 10^{-7} mm3/N-m. Adding graphene to the polymer matrix decreases the likelihood of harmful reactions including sulphide and oxides, thus providing low friction and wear activity.

Harpreet et al. [12] examined tribological actions of Al-SiC, Al-B_4C and Al-SiC-B_4C composite under lubricated condition using various solid particles, such as molybdenum disulphide (MoS_2), boric acid (H_3BO_3) and multi-wall carbon nanotubes (MWCNT) dispersed in paraffinic SN500 oil. The additives H_3BO_3 and MWCNT improve both friction and wear behavior while MoS_2 displays minimal frictional performance enhancement.

An AA7075-B4C/MoS_2 hybrid composite was prepared by Patle et al. [13] using friction stir processing (FSP). After the heat treatment (T6, solution treatment at 0.5 h at 515 °C, quenching in cold water, and artificial aging at 120 °C for 24 h) the hardness value increased from 156 to 160 HV for the hybrid composites. The presence of B_4C and MoS_2 decreases the direct interaction between the counter face and matrix material.

Panwar et al. [14] studied on redmud-reinforced tribological behaviour of Al-6061. Input variables such as ageing time, sliding distance, sliding speed, particle size and load are influenced on coefficient of friction. The results indicate that the friction coefficient is increased by greater sliding distance and decreased as a result of higher sliding speed. In addition, the friction coefficient increases first to second level, after that the load increases constantly, with the further application of higher load.

In this analysis, lamellar MoS_2 particulates are used in AMCs to improve the tribological characteristics of the composite material. Although among the major determinants, particular attention has been given to oxide minerals (i.e., Al_2O_3) as filler materials in the matrix material, owing to impact on mechanical and physical properties of composites. Similarly, this study determined the optimal tribological performance condition using process parameters such as % of Al_2O_3, % of MoS_2, sliding velocity and sliding distance, whereas the responses are wear rate and coefficient of friction.

2. FABRICATION OF COMPOSITES BY STIR CASTING PROCESS

Aluminum alloy (Table 1) is melted in a bottom pouring furnace (vide in Fig. 1a) well above its liquid temperature, i.e. 750 °C, in a graphite crucible. The crucible is used to hold the molten aluminum in the casting furnace. The particulates of Al_2O_3, and MoS_2 were preheated for 2 hours in an electric oven at 500 to 600 °C respectively, to eliminate the adsorbed artificial hydroxide coating as well as other gasses on the surface. If the metal is fully melted and temperature was set just above level of the liquidus 750 °C, then the melt is allowed to cool in between points of its liquidus and the solidus but also kept in a semi solid form. Magnesium ribbon was added into the molten metal prior to actually incorporating reinforcement to continue improving wettability. Measured volume of reinforcement has been fed into molten metal 3 to 4 times than just adding at once, and blended for 10 min in the whirlpool with help of stirrer. The mixture is again processed to a completely liquid phase once again. The furnace temperature is maintained at 760±10 °C. The melt was poured into the sand casting mold (Fig. 1b) after stirring operation.

Table 1. Chemical composition of Al-Si-Mg matrix.

Element	Si	Fe	Cr	Cu	Mn	Zn	Mg	Bal
Content (%)	1.15	0.7	0.15	0.1	0.05	0.05	0.03	Al

(a) (b)

Fig. 1. (a) Stir casting set-up (b) Cast-iron mold.

2.1 Testing methods

The primary objective of characterization in the present research is to assess the viability of composite materials in wear resistance as well as friction behavior of hybrid matrix composites. The characterization methods being used are: Vickers micro hardness test, surface morphology examination (metallurgical microscope, XRD, SEM), density calculation, and pin-on - disk wear test and friction calculation coefficient. Archimedes principle has been used to measure the densities of a stir cast hybrid reinforced aluminium matrix composite materials that offers a precise and faster process for assessing the density of many abnormal solid particles.

Optical microscope has been used to examine the metals structure at scales ranging and provide a descriptive and analytical characterization. In this study a metallurgical microscope is used to analyze the shape, size, and scattering of structure oxide fillers. While analyzing the structure of hybrid matrix material, the samples are well polished using fine grade grit and then graded for 20-40 seconds with a Keller test solution (1 ml hydrofluoric acid, 1.5 ml hydrochloric acid, and 2.5ml nitric acid in 95ml distilled water).

Fig. 2a shows the set up of pin-on–disk test rig. Fig. 2b shows the fractured tensile samples. The wear pin specimens cut out from the composite metals with a 35 mm length and 8 mm diameter, shown in Fig. 2c. The Pin

specimens were polished with a fine sandpaper of grades 800 and 1200 before carrying test. The wear test was conducted in compliance with ASTM standards G99-95a. The counter Disk content was EN32. The disk was up to 80 mm in diameter, and 8 mm in thickness. The tests were conducted at a constant sliding distance of 1500 m. Pre and post wear testing, the pin and disk is cleaned by acetone. The weight loss of specimen is converted to volume loss and aid of wear rate with specified time of abrasion. The frictional forces are acquired from test, which are used to calculate coefficient of friction. The worn-out and sub surfaces/particles were examined with scanning electron microscope (SEM) and Energy-dispersive X-ray spectroscopy (EDS) analyses.

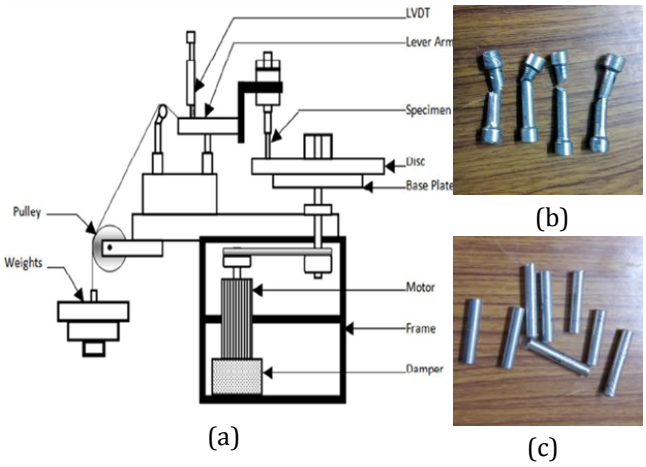

Fig. 2. (a) Pin-on-disc setup (b) Fractured tensile samples (c) Wear test samples.

2.2 Taguchi method

As per the complete factorial design, it is too difficult to perform a set of experiments once the number of process variables and its levels are higher. The Taguchi method provides a good design of conventional orthogonal arrays to solve the problem that also helps to evaluate all this parameter except for restricted experiments. Taguchi's methods consist of an exploratory approach to get knowledge about a process's behaviour. Further the results are evaluated through variance analysis. ANOVA is a basis for assessing the significant factor and quantifying the variance into recognizable deviation causes. The F-test is a ratio of variances in samples [15–18].

Comparing a source's F-ratio to the tabulated F-ratio is called the F-test. When Variance Analysis was conducted on even a set of statistics and the corresponding square sums computed, this data could be used to allocate the adjusted square sums to the relevant variables. The percentage of contribution in each variable is given by contrasting this value with the overall sum of squares. P-value (significance probability) is being computed according to the significance of F. If P-value for a term also seems to be less than 0.05 (For 95 % level of confidence), then it will be observed that the impact of variables / factor interaction upon its chosen response is significant.

3. RESULT AND DISCUSSIONS

3.1 Characterization of self-lubricating composite

The self-lubricated MoS_2 particles are shown in Fig. 3(a), and there is proof that the matrix was effectively penetrated by hollow particles. Spectrum of EDS in Fig. 3 (b) shows the elements Mo, S, O and Al peaks arising from the underlying substrate. The XRD plot (vide in Fig. 4) of exhibited the presence of various compound Al-Si-Mg/Al_2O_3/MoS_2 composite. The XRD pattern is confirmed the presence of MoS_2 at a bragg angle of 14° due to stacking fault energy and avail in the form of layered structure. By considering other peaks, noticed that formation of a strong bonding between compounds, which helps to increase in wear resistance of composite.

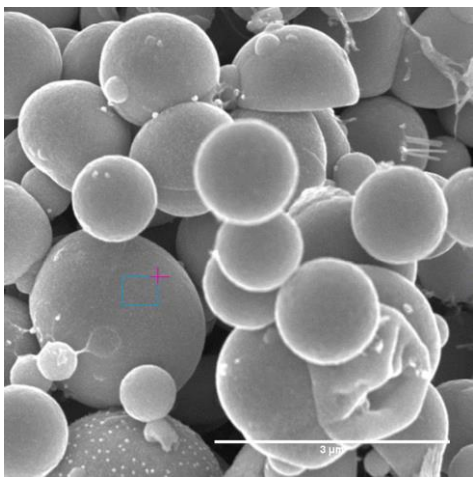

(a)

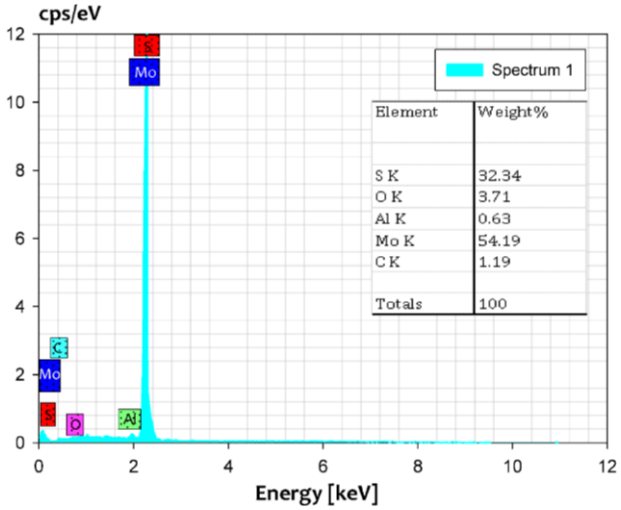

(b)

Fig. 3. (a) MoS_2 particles (b) EDX of MoS_2 particles.

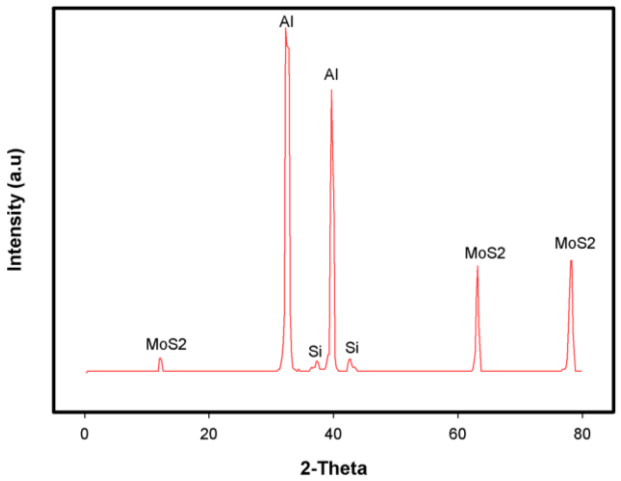

Fig. 4. XRD plot of Al-MoS_2 composite.

3.2 Mechanical properties of cast-composites

Fig. 5 (a, b, and c) shows the hardness of composites increased with the increasing content of Al_2O_3 and MoS_2, owing to the hard phase (Al_2O_3) compounds, and uniform distribution of reinforced particles in the composites. Fig. 5(a) revealed that the trend of tensile strength and harness values having indirectly characters to each other. Fig. 5(b), mono-reinforced (16% Al_2O_3) composite exhibited better hardness compared to base matrix, hybrid (Al_2O_3 and MoS_2) composite. Fig. 5(c) revealed hybrid composite hardness and tensile strength increased with increasing of Al_2O_3. The hardness of composites may be increased due to coefficient of thermal expansion (CTE), the particles of MoS_2 (8.43 m/m°C) is less than that of base alloy (22.3 m/m°C).

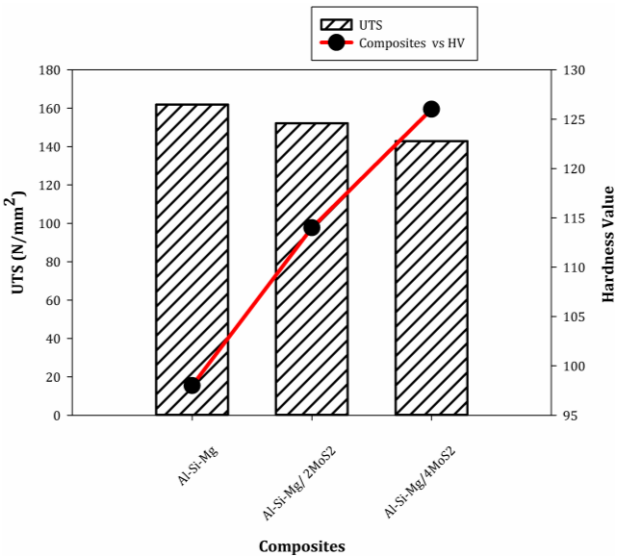

(a)

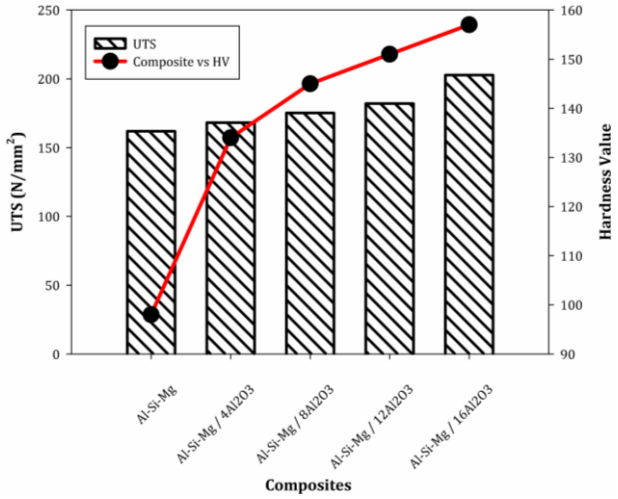

(b)

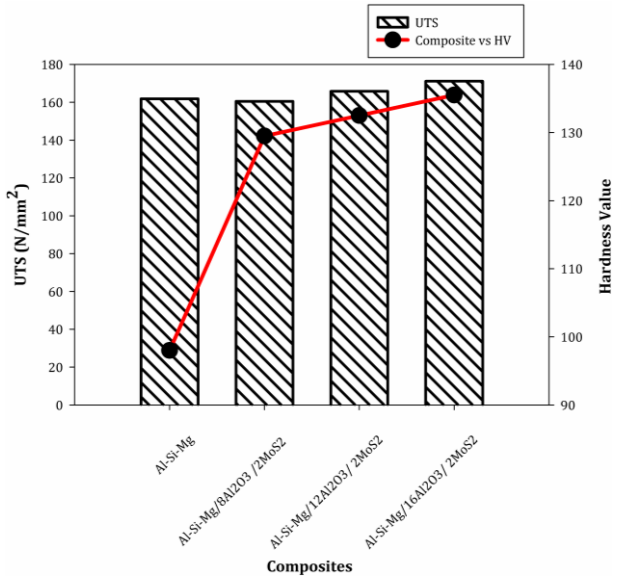

(c)

Fig. 5. Mechanical properties of (a) Al-MoS_2 composites, (b) Al-Al_2O_3 composites, (c) Hybrid (Al-MoS_2 -Al_2O_3) composites.

Therefore, during the solidification process, a large number of dislocations are created at the particle-matrix interface, which further increases the hardness of the matrix. The tendency of mono-reinforced (Al_2O_3, vide in Fig. 5b) and hybrid (Fig. 5c) composite, while increasing Al_2O_3 hardness and tensile strength were increased. Correspondingly, the ultimate tensile strength (UTS) (vide in Fig. 5a) considerably decreased in addition to MoS_2, thereby 6.02 and 11.75% as compared to base matrix, owing to MoS_2 are layered structure and soft in form.

However, Al/16%Al_2O_3 (Fig. 5b) and hybrid composite i.e., Al-Si/2%MoS_2/16%Al_2O_3 (Fig.5c) strength increased by 25.22% and 5.07% respectively. This decrease in UTS may be due to particle pull-out and crack propagation in composites as well lower UTS of MoS_2 (≈70MPa) compared to the base matrix(162 MPa), which results in decreased UTS in hybrid composites as compared to mono composites.

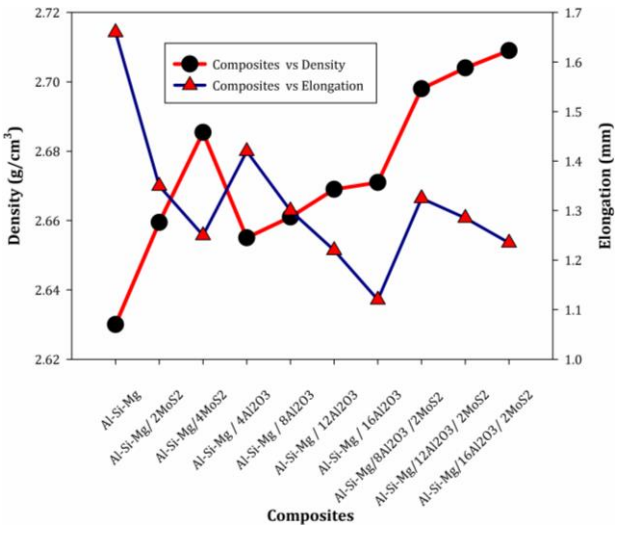

Fig. 6. Properties of composites: (a) Density, (b) Elongation.

The density of Al_2O_3 particulate (3.92 g/cm^3) is higher than the base alloy (2.63 g/cm^3) and hence the increase in Al_2O_3 content in Al matrix will increase the density of the composite. The density of MoS_2 particulate (5.01 g/cm^3) is higher than the aluminium alloy; and due to this, the increase in reinforcement (such as Al_2O_3 and MoS_2) weight percentage will increase the density of the hybrid composites and was found maximum in Fig. 6. It can be observed in Fig. 6, the density of mono composites (i.e., Al/2% MoS_2 and Al/4%MoS_2) are increased by 1.12 and 2.11% as compared to base alloy. Similarly, the density of Al_2O_3 composites increased with increasing weight % of Al_2O_3. The hybrid composites (i.e., Al/2%MoS_2/ 16%Al_2O_3) is increased by 3.01% compared to base matrix.

The elongation of the composites shows in Fig. 6 a marginal decrease than base alloy indicating that the addition of reinforcement (Al_2O_3 and MoS_2) lowered the ductility of the composite. With addition of MoS_2, the composites such as 2% and 4% wt% of MoS_2 elongation were decreased by 18.67 and 24.70% compared to base alloy. Also, 16% Al_2O_3, and 2%MoS_2/16%Al_2O_3 resulted in a decrease in %elongation by 32.53% and 25.59% respectively. This attribute increases the hardness of composites.

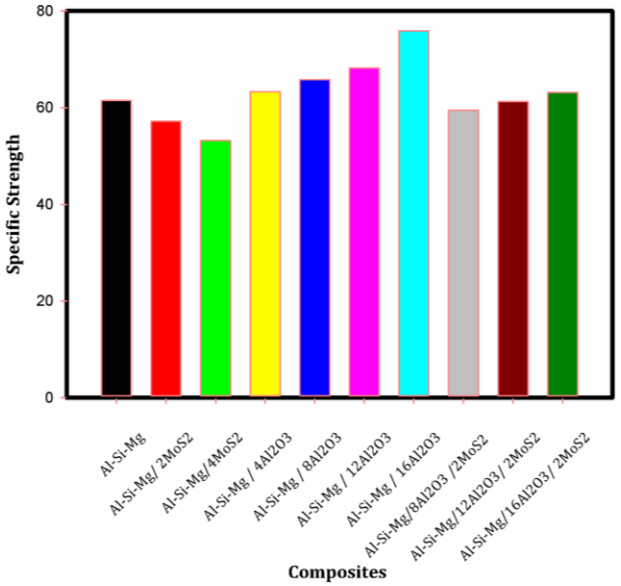

Fig. 7. Specific strength of Al-Si-Mg/MoS2/Al2O3 composites.

Precisely, a conclusion from (Fig. 7) the specific strength of Al-Si/4%MoS_2 exhibited least and Al-Si/16%Al_2O_3 composite exhibited the best as compared to other composites.

3.3 Microstructural examination

The optical micrographs of unreinforced aluminium alloy as well as those of composites (Fig. 8(a-i)) show as cast (dendritic) structure consisting of Al_2O_3 particles. The microstructure of the composites (Al-Si-Mg/12Al_2O_3 and Al-Si-

Mg/16Al_2O_3) shows the increasingly fine grain structure, due to heterogeneous nucleation caused by the addition of Al_2O_3. Stirring effect along with the addition of magnesium in the melt increases wettability, resulting in a better distribution of particles. Relatively lower porosity in the casting, an important element of fabricated composite materials, are other features of the microstructure. During solidification of the composites and particles rejected by the solid-liquid interface, aluminium dendrites solidify first to segregate into the interdendritic zone [19]. Optical micrographs show the microstructures of Al-Si-Mg alloy (Fig. 8a), Al-Si-Mg/8Al_2O_3/2MoS_2 (Fig. 8g), Al-Si-Mg/12Al_2O_3/2MoS_2 (Fig. 8h) and Al-Si-Mg/16 Al_2O_3/2MoS_2 (Fig. 8i) hybrid composites.

In general, grains are much finer for the cast composite in comparison to Al-alloy (Fig. 8a) due to chilling of casting and enhanced heterogeneous nucleation owing to incoherent particles in the material inducing higher nucleation rate. Fine grains increase the hardness and tensile strength of as cast composite. The volume fraction is also measured by image process analyzer and is cited in Fig. 9. The phase-1 (yellow colour) represents % of Al_2O_3 and phase-2 (blue colour) represents base matrix.

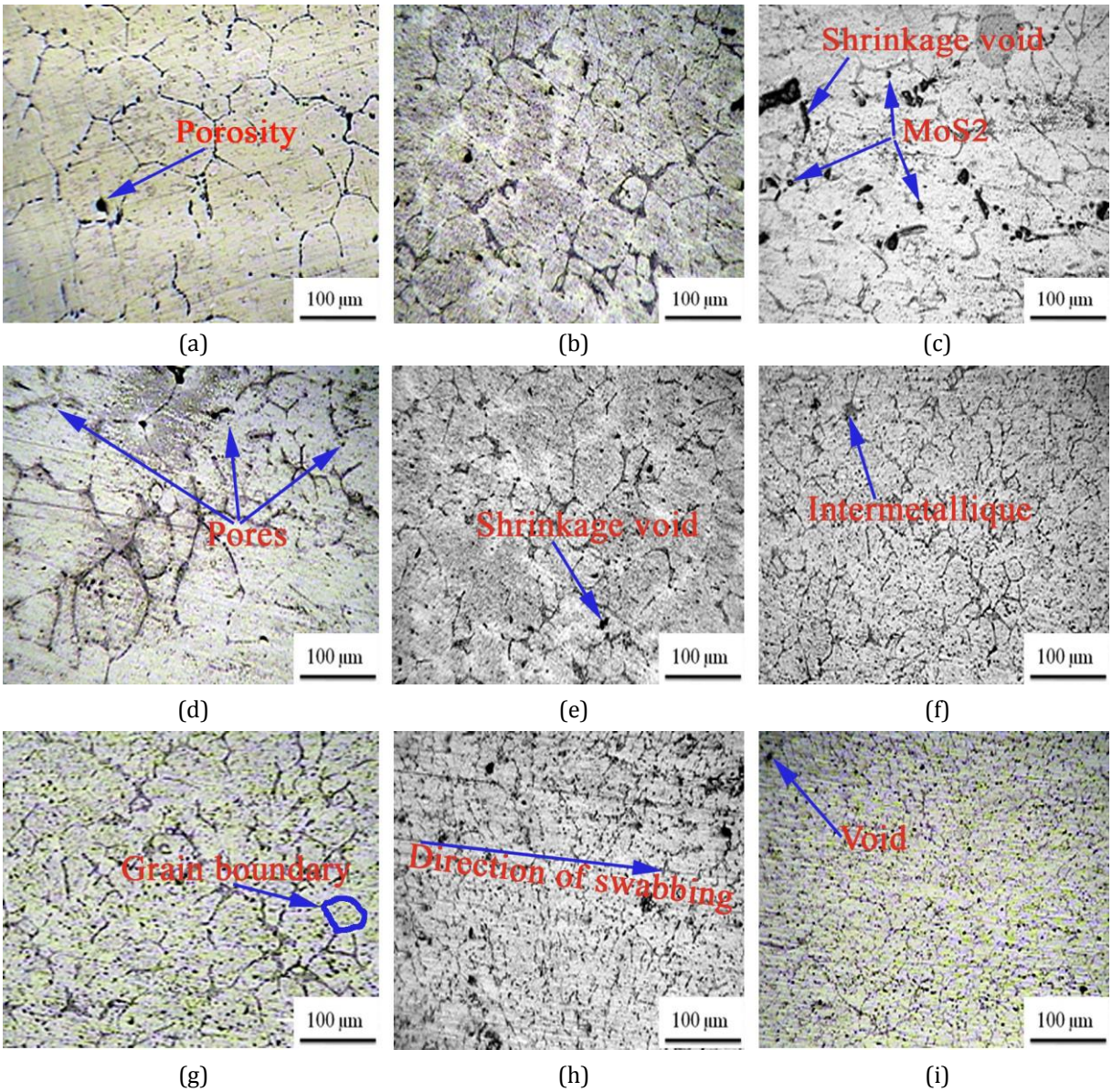

Fig. 8. Microstructure of composites (a) Al-Si-Mg, (b) Al-Si-Mg/2MoS_2, (c) Al-Si-Mg/4MoS_2, (d) Al-Si-Mg/4Al_2O_3, (e) Al-Si-Mg/8Al_2O_3, (f) Al-Si-Mg/12Al_2O_3, (g) Al-Si-Mg/2MoS_2/8Al_2O_3, (h) Al-Si-Mg/2MoS_2/12Al_2O_3, (i) Al-Si-Mg/2MoS_2/16Al_2O_3.

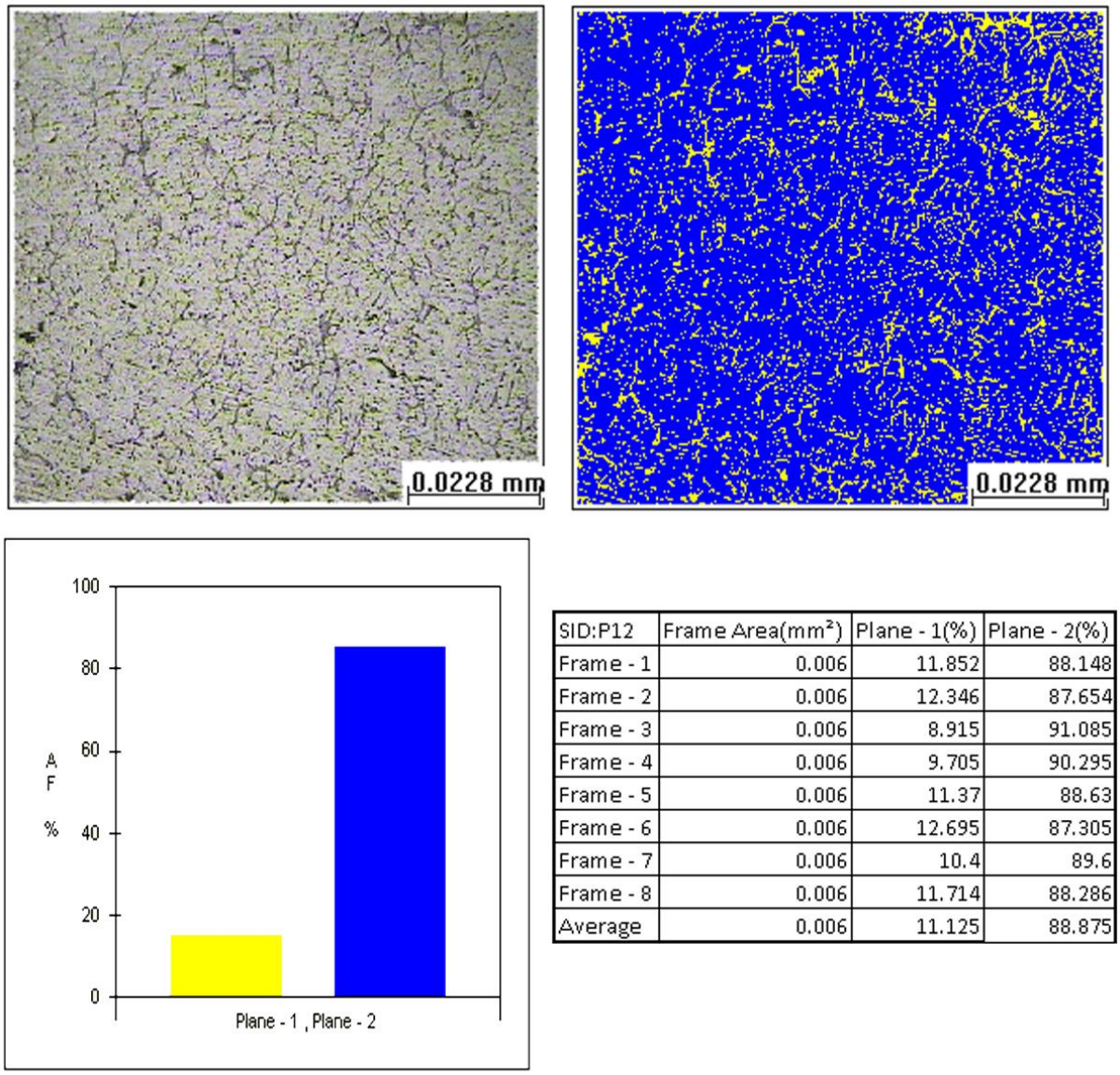

SID:P12	Frame Area(mm²)	Plane - 1(%)	Plane - 2(%)
Frame - 1	0.006	11.852	88.148
Frame - 2	0.006	12.346	87.654
Frame - 3	0.006	8.915	91.085
Frame - 4	0.006	9.705	90.295
Frame - 5	0.006	11.37	88.63
Frame - 6	0.006	12.695	87.305
Frame - 7	0.006	10.4	89.6
Frame - 8	0.006	11.714	88.286
Average	0.006	11.125	88.875

Fig. 9. Volume fraction and distribution of reinforced particles in Al- Al_2O_3 composites.

3.4 Investigation on fracture behaviour of composites

Detailed Scanning Electron Microscopic (SEM) investigations were carried out on tensile test specimens to study the fracture behaviour of composites as well as the influence of increasing reinforcement content. From the Micrographs it is possible to detect broken particles around the ductile areas with fine, almost non-circular dimples, known as "tear cords" and matrix interfaces with decohesion – particular interfaces. Fig. 10 (a-d) shows the SEM fractograph of Al-Si-Mg, Al-Si-Mg/2MoS_2 and AlSi10Mg/16Al_2O_3, Al-Si-Mg/2MoS_2/16Al_2O_3 respectively.

The aluminium matrix alloy fracture was primarily fibrous showing microscopic void formation, their progressive growth and final coalescence around the reinforcement particles. It can be further observed that while the unreinforced alloys show predominantly ductile fracture (fibrous regions), the composite specimens show increasing mixed mode (ductile and brittle regions). Fractograph studies also reveal features such as particle pull-out, crack growth and propagation, which promote fracture. Fracture of Al_2O_3 occurred, mainly in the Al-Si-Mg/16Al_2O_3 (Fig. 10c) based composite, but in Al-Si-Mg/2MoS_2 (Fig. 10b) based composites clearly showed interfacial debonding.

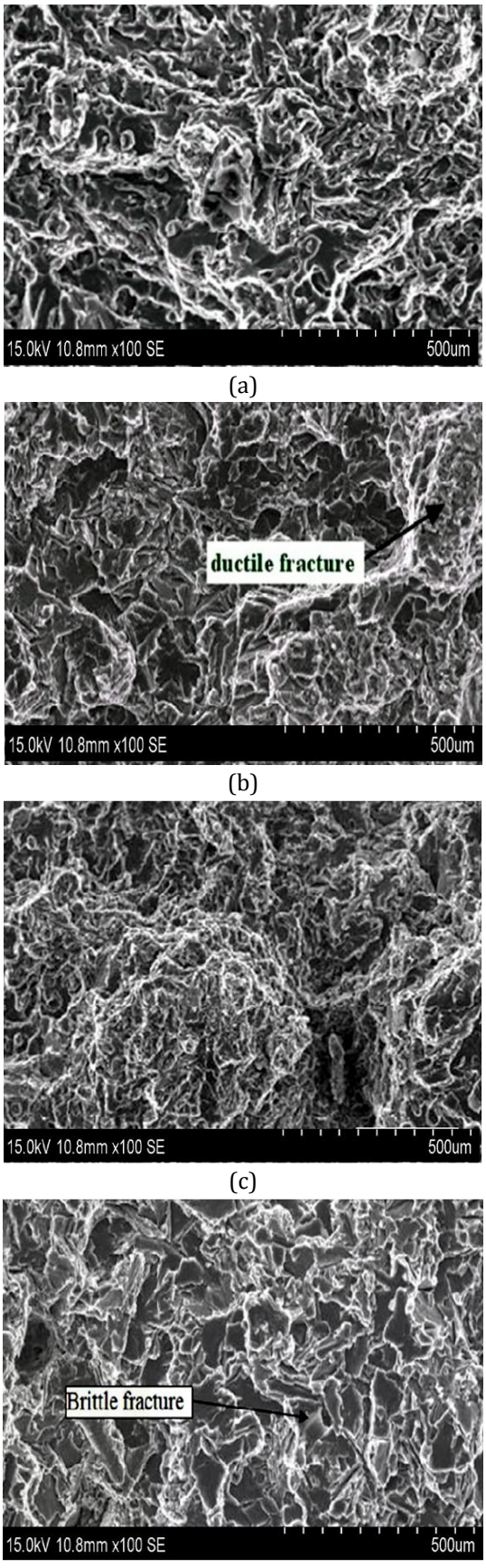

Fig. 10. Fracture tensile samples of composites (a) Al-Si-Mg, (b) Al-Si-Mg/2MoS_2 (c) Al-Si-Mg/16Al_2O_3, (d) Al-Si-Mg/ 2MoS_2/16Al_2O_3.

The fracturing and debonding of particles in both composites caused large voids and dimples, while the small ductile dimples can be attributed either to the limitations of the plastic flow of the aluminium matrix or to the reduction of strains induced by the cracking of particles leading to the formation of tear ridges. Fig. 10d shows that in Al-Si-Mg/2MoS2/16Al2O3 composites, relatively little plastic deformation took place before fracture. As a result of tensile stress acting natural to the plane with weak bonding, fracture occurred by cleavage [20,21]. The higher dislocation density is another explanation for brittle fractures. The fact that plastic deformation occurs by the movement of dislocations may explain this. When dislocations increase in a material due to stresses above the yield point, since they pile up at barriers, it becomes increasingly difficult for the dislocations to pass. A material that already has a high dislocation density can therefore only deform in a brittle way a little before it fractures. Yet the grain size is another factor affecting the fracture behaviour. The fracture becomes more brittle as the grains get smaller. This is because dislocations have less room to travel in minor grains before they meet a grain boundary, thereby reducing plastic deformation. Thus, fractures in the hybrid composites are relatively more brittle in nature. Similar results were reported in the case of Al alloy / hybrid composites, where the UTS and Young's modulus of the composite increased while increase in particle volume fraction increased the strength, but decreased the ductility of the composites.

3.5 Analysis of variance (ANOVA)

In the present analysis, the tribological quantities such as wear rate and friction coefficient are primarily regulated by four factors at three levels shown in Table 2. The test plan is composed of 27 tests shown in Table 3. The chosen orthogonal array has been the three-level L27 (3^{13}), with 27 rows and 13 columns. The composition of Al_2O_3 and MoS_2, load, as well as sliding velocity of the four variables are allocated respectively in a column of 1, 2, 5, 9 and the remaining columns are allocated in the interactions.

Table 2. Factors with their levels.

Run	Al_2O_3 (A)	MoS_2 (M)	Sliding Velocity (SV)	Load (L)
1	8	0	1	10
2	8	0	1.5	20
3	8	0	2	30
4	8	2	1	20
5	8	2	1.5	30
6	8	2	2	10
7	8	4	1	30
8	8	4	1.5	10
9	8	4	2	20
10	12	0	1	20
11	12	0	1.5	30
12	12	0	2	10
13	12	2	1	30
14	12	2	1.5	10
15	12	2	2	20
16	12	4	1	10
17	12	4	1.5	20
18	12	4	2	30
19	16	0	1	30
20	16	0	1.5	10
21	16	0	2	20
22	16	2	1	10
23	16	2	1.5	20
24	16	2	2	30
25	16	4	1	20
26	16	4	1.5	30
27	16	4	2	10

Table 3. Design of experimental runs (L27) and responses with S/N ratios.

Run	WR (mm3/m)*10-3	CF	SN of WR	SN of CF
1	2.605	0.262	-8.31	11.63
2	2.660	0.276	-8.50	11.18
3	2.703	0.290	-8.64	10.76
4	2.989	0.277	-7.84	11.14
5	3.004	0.291	-7.89	10.72
6	1.663	0.247	-1.14	12.16
7	3.476	0.293	-9.21	10.67
8	1.987	0.248	-2.92	12.10
9	2.070	0.262	-3.42	11.64
10	2.467	0.222	-9.51	13.07
11	2.482	0.236	-9.55	12.55
12	1.141	0.219	-4.42	13.19
13	2.851	0.247	-9.10	12.13
14	1.362	0.193	-2.68	14.30
15	1.445	0.207	-3.20	13.70
16	1.754	0.194	-4.55	14.23
17	1.809	0.208	-4.83	13.64
18	1.852	0.218	-5.04	13.23
19	2.889	0.214	-10.82	13.39
20	1.400	0.194	-5.96	14.24
21	1.483	0.186	-6.32	14.61
22	1.689	0.163	-4.88	15.76
23	1.744	0.176	-5.15	15.09
24	1.787	0.208	-5.35	13.64
25	2.176	0.172	-6.75	15.29
26	2.191	0.168	-6.81	15.49
27	0.850	0.164	1.41	15.70

According to the principle that level of flexibility will be approximately equal to a number of certain processing variables after a factorial design. It consists of a 26 degree of freedom in an orthogonal array of L27. The degree of freedom is based on a number of levels minus one in each factor. The total degree of freedom required for the entire experiment is determined by the number of variables, levels, and their interactions.

3.6 Analysis of wear rate

The effect of each individual parameter is represented by means of response table and response graph. The response table is prepared for each level of parameters by calculating the average value in terms of S/N ratios and is shown in Table 4. Based on the mean values from the response table, response graphs are plotted and shown in Fig. 11. The significance of each control factor is indicated by the largest delta value [22]. Accordingly, the load (L) is the most significant parameter followed by sliding velocity and percentage of MoS_2. The optimal parameter combination for minimum wear rate is A3M3SV3L1.

Table 4. Response table of wear rate for S/N ratio.

Level	Al_2O_3 (A)	MoS_2 (M)	SV	Load (L)
1	-6.431	-8.004	-7.887	-3.718
2	-5.877	-5.249	-6.034	-6.168
3	-5.626	-4.681	-4.013	-8.047
Delta	0.805	3.322	3.875	4.329
Rank	4	3	2	1

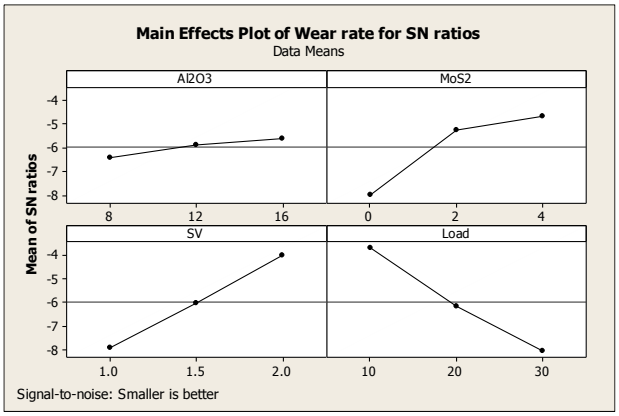

Fig. 11. Optimal condition of wear rate for signal to noise ratio.

The same can also be observed, from the response graph (Fig. 11). Using multiple linear regressions, the model for wear has been developed in terms of A, M, SV and L is given Eq. (1):

$$WR=3.098 -0.0231 A-0.193 M-0.878 SV+0.049 L \quad (1)$$

The residuals appear to follow a straight line from the wear rate data shown in Fig. 12. So, it is proof of no non-normality, skewness, outliers, or unidentified variables in existence. The residuals should be randomly dispersed around zero and the range of -1 to +1. The residuals do not appear to be randomly scattered around zero. It shows non-constant variance, there are missing terms, outliers, or influential points, and the probability slope is y = 0.0219x + 0.9984, R^2 = 0.9707. From Fig. 12, the histogram shows the distribution is centred on -0.8 to 0.6 and its shape is almost symmetrical. Values range frequency from 0.75 to 6. Moreover, the histogram has been compared to the fitted normal distribution and it suggested with good fit. Residuals versus order of response signal to noise ratio data indicates either there are systematic effects in the data due to time or data collection order. The residuals lay randomly in between -0.8 to 0.8 from the centre line. From Fig. 9, run 14 has high residual i.e. -0.755 is exhibited below the centre line. Similarly, run 22 and 7 contain more residual and displayed above the centre line.

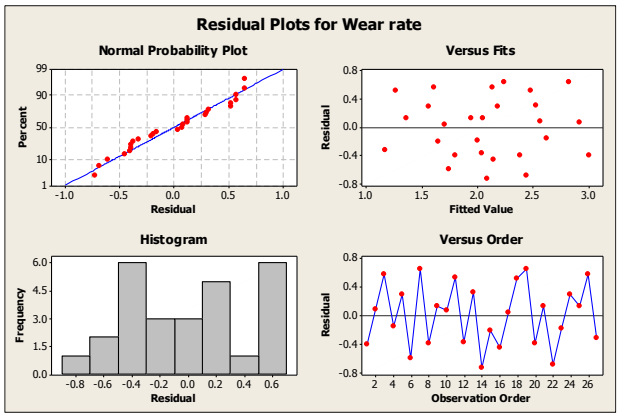

Fig. 12. Residual plots of wear rate for signal to noise ratio.

From the ANOVA (Table 5), load (38.95%) is the most influential parameter followed by sliding velocity (31.04%). It observed from P-values, process parameters such as M, SV and L are significant, whereas A is insignificant. The combined factors don't have a great effect on wear rate. The contributions of overall factors are performed 98.6% of the total variance in wear rate.

Table 5. Analysis of variance for wear rate.

Source	DF	Seq SS	Adj MS	F	P	% Contr.
A	2	3.057	1.528	2.99	0.125	1.40
M	2	56.845	28.423	55.68	0	26.10
SV	2	67.606	33.803	66.23	0	31.04
L	2	84.839	42.419	83.11	0	38.95
A*M	4	0.670	0.168	0.33	0.85	0.31
A*SV	4	0.975	0.244	0.48	0.752	0.45
A*L	4	0.748	0.187	0.37	0.825	0.34
Error	6	3.063	0.510			
Total	26	217.803				
S = 0.7144 R-Sq = 98.6% R-Sq(adj) = 93.9%						

3.7 Analysis of coefficient of friction

From Table 6, the percentage of MoS_2 is the most significant parameter followed by load and sliding velocity. The optimal parameter combination for minimum coefficient of friction is A3M3SV2L1. The same can also be observed from the response graph which is shown in Fig. 13. The effect of parameters such as A, M and SV having a trend increased with decreasing coefficient of friction.

Table 6. Response table of coefficient of friction for S/N ratios.

Level	Al_2O_3	MoS2	SV	Load
1	13.56	11.33	13.49	14.59
2	13.73	13.49	13.73	13.7
3	13.92	16.38	13.98	12.9
Delta	0.36	5.04	0.49	1.69
Rank	4	1	3	2

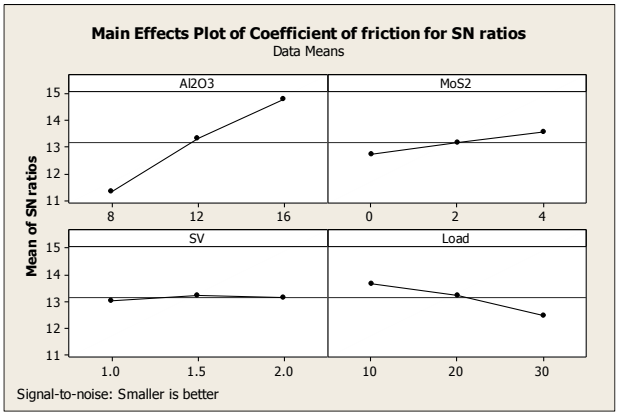

Fig. 13. Optimal condition of coefficient of friction for signal to noise ratio.

Using multiple linear regressions, the model for wear has been developed in terms of A, M, SV and L is given Eq. (2)

$$CF=0.273 -0.0024 A-0.022 M-0.005 SV+0.016 L \quad (2)$$

From the ANOVA (Table 7), MoS_2 (88.23%) is the most influential parameter followed by load (9.81%). The contributions of overall factors are performed 99.70% of the total variance in coefficient of friction. It is observed from P-values, process parameters such as M, SV and L are significant.

Table 7. Analysis of variance for coefficient of friction.

Source	DF	Seq SS	Adj MS	F	P	% Contr.
A	2	0.591	0.295	4.19	0.073	0.45
M	2	115.191	57.596	816.42	0	88.23
SV	2	1.103	0.551	7.82	0.021	0.84
L	2	12.813	6.406	90.81	0	9.81
A*M	4	0.039	0.010	0.14	0.961	0.03
A*SV	4	0.367	0.092	1.3	0.368	0.28
A*L	4	0.035	0.009	0.12	0.968	0.03
Error	6	0.423	0.071			
Total	26	130.562				
S=0.2656		R-Sq(adj) =98.60%			R-Sq=99.70%	

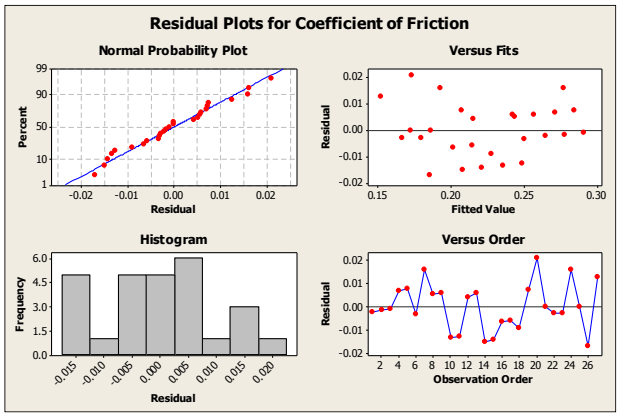

Fig. 14. Residual plot of coefficient of friction for signal to noise ratio.

Fig. 14 shows data of coefficient of friction, the residuals appear to follow a straight line. So, it is evidence of no existence of non-normality in variables. The residuals should be uniformly distributed around zero. Based on this plot, the residuals do not appear to be randomly scattered about zero within the range of -0.02 to 0.02. It is evidence of non-constant variance, missing terms, outliers, or influential points exist and the slope of probability is y = 0.0014x + 0.1538, R^2 = 0.985. From Fig. 14, the histogram shows the distribution is centred on -0.015 to 0.020 and its shape is almost symmetrical. Values range frequency from 0 to 6. Moreover, the histogram has been compared to the fitted normal distribution and it suggested with good fit. The residuals lay randomly in between -0.02 to 0.02 from the centre line. From Fig. 14, run 20 has high residual i.e. 0.0198 is exhibited above centre line. Similarly, run 26 and 7 have more residual and displayed above the centre line.

3.8 Confirmation test

Confirmation evaluation was carried out to corroborate the numerical analysis by choosing test conditions that are different from those used in the analysis. Table 8 offers the variables used in the confirmation test. With the estimated values developed from the regression equation, tentative results are evaluated. Table 8 shows that, with the least error (±5 percent), the experimental values and calculated values from the regression equation are nearly the same. The resulting equations are able to predict the roughness of the surface to an acceptable level of precision.

Table 8. Confirmation test combination with validation of responses.

Test Parameters			
Al_2O_3	MoS_2	SV	Load
8	2	1.25	30
12	2	1.25	30
16	2	1.25	30

Wear rate		
CAL	EXP	ERR
2.893	2.912	0.65
2.801	2.755	-1.68
2.709	2.837	4.54

Coefficient of friction		
CAL	EXP	ERR
0.250	0.245	-2.2
0.240	0.255	5.67
0.231	0.242	4.43

4. TRIBO SURFACE EXAMINATION USING SEM

The worn surface (vide in Fig. 15) of alloy/composites are tested at a sliding velocity of 1.5 m/s, load of 30 N, and sliding distance of 900 m.

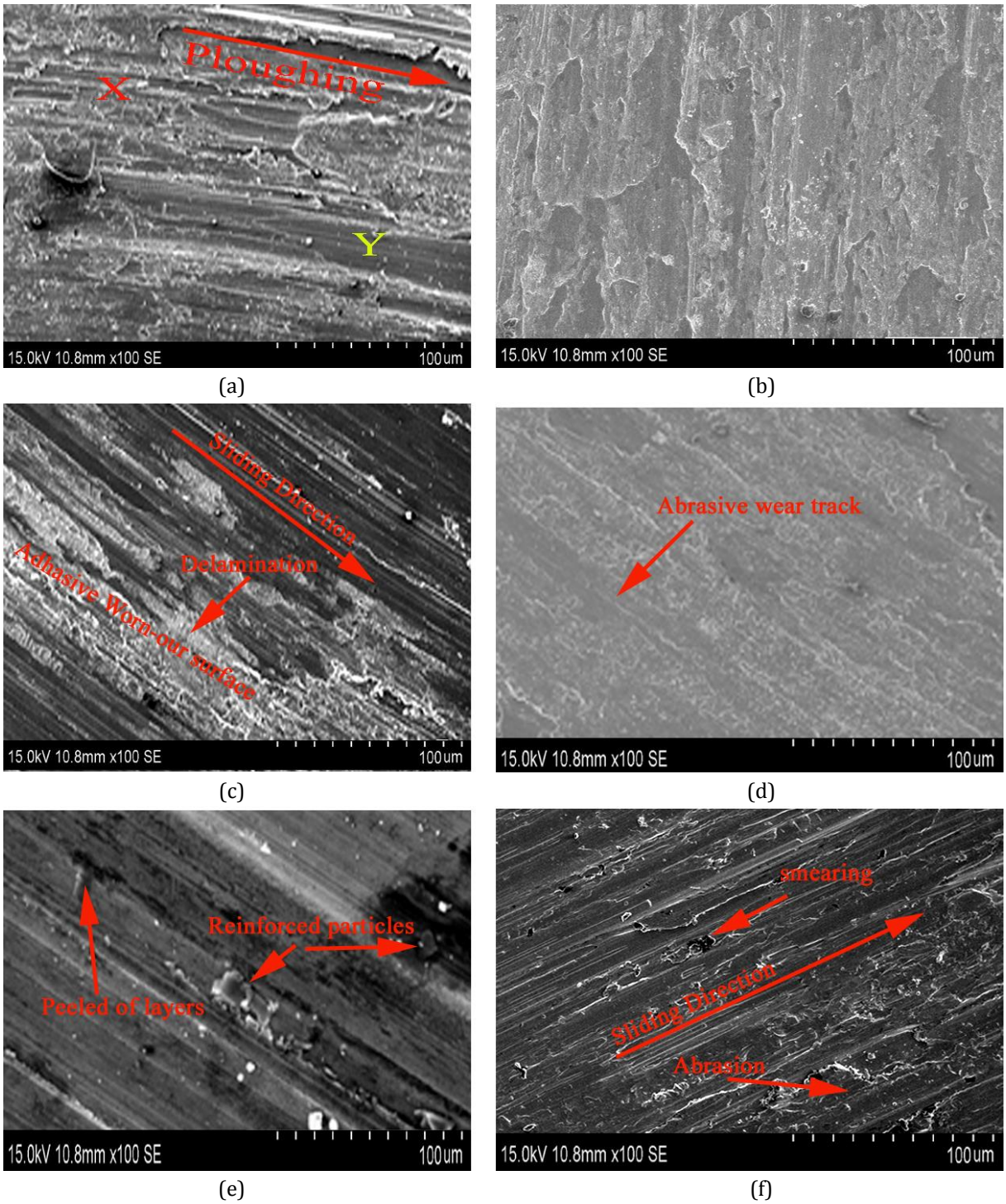

Fig. 15. Worn-out surfaces of composites: (a) Al-Si-Mg, (b) Al-Si-Mg/2MoS_2, (c) Al-Si-Mg/4Al_2O_3, (d) Al-Si-Mg/12Al_2O_3, (e) Al-Si-Mg/2MoS_2/8Al_2O_3, (f) Al-Si-Mg/2MoS_2/12Al_2O_3.

The worn surface of base alloy (Fig. 15a) evidently shows two mechanisms such as abrasion (Mark 'X') and adhesion (Mark 'Y'). Abrasion (Mark 'X' in Fig. 15a) revealed as deep grooves, presence of large debris on the worn surface, , large burrs size at the edge, plastic deformation caused an increased wear rate. The second mechanism is abrasion (Mark 'Y' in Fig. 15a), which represents red colour and owing to high temperature between tribo surfaces. The worn surface morphology of the Al-alloy/2MoS_2 composite is shown in Fig. 15b. The surface noticeably shows that the wear pattern, micro cutting, very fine debris and burr at the edge of the surface. It is due to the MoS_2 tribo layer between the contacting pairs and forms an adherent film between the contact surfaces so that it leads to decrease the plastic deformation on the pin sample. A sharp

delaminated layer is observed on the worn surface, which separates the contacting pair and causes reduction in a wear rate.

The tribo surface of the Al-alloy/4Al_2O_3 (Fig. 15c) composite is mainly worn out on the surface of the pin due to the ploughing and fracture of oxide particles of Al_2O_3. The worn surface indicates the existence of detachment and abrasion of material near the contacting surface. The main reasons of the severe plastic deformation are contact between the pairs, low hardness and ductile behavior of Al. Fig. 15d shows a smoother surface as compared to Al-alloy/4Al_2O_3. While increasing in % of Al_2O_3, the particles are squeezed out from the matrix and mating lay on the disc, and also smeared particles formed a layer in contact interface i.e., Mechanically Mixed Layer (MML) acts as load bearer [23–25]. The layer reduces the coefficient of friction at a lower speed and at a higher speed the layer breaks, and it leads to an increased coefficient of friction. It is also observed in Fig. 15e, there is a large severe plastic deformation as compared to other hybrid composite (Fig. 15f). The worn surface of a hybrid Al-alloy - 2MoS_2-12%Al_2O_3 composites is changed due to the reinforcement of Al_2O_3 and MoS_2 lubricant. It is observed that the surface of the composite was smooth with small grooves and fine debris. The burr size at the edge of the worn surface is very small as compared to base matrix.

5. CONCLUSIONS

In this research work, Al-Si-Mg/MoS_2/Al_2O_3 composites were fabricated using the stir-casting technique and the mechanical and tribological characteristics were studied, which are highlighted as follows

- With an addition of MoS_2 particles, properties such as hardness, elongation and specific strength decreased whereas Tensile strength and density were increased.
- A trend of increased in mechanical and tribological properties with addition of Al_2O_3 particles to Al-Si-Mg.
- The microstructure of the composites shows the increasingly fine grain structure, due to heterogeneous nucleation caused by the addition of Al_2O_3.
- The fracture behaviour of composites are influencing on % of reinforcement contents. MoS_2 content fractograph represents ductile behavior whereas hybrid composite (Al-Si-Mg/2MoS_2/16Al_2O_3) exhibited brittle in nature.
- The optimal parameter combination for wear rate is A3M3SV3L1.
- The optimal parameter combination for coefficient of friction is A3M3SV2L1.
- The Fractographs, worn-out surfaces of the composites were analysed with scanning electron microscope (SEM).

Acknowledgement

The author would like to thank to Dr. Hota Ravisankar (HOD, Dept. of Mechanical Engineering, GITAM University, Vizag and A.P) for their kind support and act as mentor in my professional carrier. However, I heard shocking news of his premature death due to Covid-19 on May 4, 2021. I felt a genius fell down and put their family and me in great trouble. I always remember your words to enhancing my carrier and support to other in a decent manner. You are one of the best teacher, researcher, and a good human being in the institute. I made a stronger individual by your leadership, mentorship, and encouragement. I am going to remember it forever. Can Our Soul Teacher Rest in Peace. I also great thankful to the editorial members of Tribology in Industry, for providing me an opportunity to gave acknowledgment to my professor.

REFERENCES

[1] P. Naresh, S.A. Hussain, B.D. Prasad, *Analysis of dry sliding wear behaviour of AA-7068/TiC MMCs*, International Journal of Materials Engineering Innovation, vol. 11, no. 1, pp. 1–19, 2020, doi: 10.1504/IJMATEI.2020.104788

[2] Y. Sahin, *Abrasive wear behaviour of SiC/2014 aluminium composite*, Tribiology International, vol. 43, iss. 5-6, pp. 939–943, 2010, doi: 10.1016/j.triboint.2009.12.056

[3] H. Ahlatci, T. Koc, E. Candan, *Wear behaviour of Al/(Al2O3p+SiCp) hybrid composites*, Tribology International, vol. 39, pp. 213–220, 2006, doi: 10.1016/j.triboint.2005.01.029

[4] R.S.S Raju, M.K. Panigrahi, R.I. Ganguly, G.S. Rao, *Tribological behaviour of Al-1100-coconut shell ash (CSA) composite at elevated temperature*, Tribology International, vol. 129, pp. 55–66, 2019, doi: 10.1016/j.triboint.2018.08.011

[5] M. Singh, B.K. Prasad, D.P. Mondal, A.K. Jha, *Dry sliding wear behaviour of an aluminium alloy – granite particle composite*, Tribology International, vol. 34, iss. 8, pp. 557–567, 2001, doi: 10.1016/S0301-679X(01)00046-9

[6] K.P. Furlan, J.D.B. de Mello, A.N. Klein, *Self-lubricating composites containing MoS2: A review*, Tribology International, vol. 120, pp. 280–298, 2018, doi: 10.1016/j.triboint.2017.12.033

[7] V. Suresh, N. Hariharan, S. Paramesh, M.P. Kumar, P.A. Prasath, *Tribological behaviour of aluminium/boron carbide (B4C)/graphite (Gr) hybrid metal matrix composite under dry sliding motion by using ANOVA*, International Journal of Materials and Product Technology, vol. 53, no. 3/4, pp. 204–217, 2016, doi: 10.1504/IJMPT.2016.079194

[8] R. Jojith, N. Radhika, *Mechanical and tribological properties of LM13/TiO2/MoS2 hybrid metal matrix composite synthesized by stir casting*, Particulate Science and Technology, vol. 37, iss. 5, pp. 566–578, 2019, doi: 10.1080/02726351.2017.1407381

[9] K.S. Vinoth, R. Subramanian, S. Dharmalingam, B. Anandavel, *Mechanical and tribological characteristics of stir-cast Al-Si10Mg and self-lubricating Al-Si10Mg/MoS 2 composites*, Materiali in Tehnologije, vol. 46, iss. 5, pp. 497–501, 2012.

[10] S. Gugulothu, V.K. Pasam, *Performance Evaluation of CNT/MoS2 Hybrid Nanofluid in Machining for Surface Roughness*, International Journal of Automotive and Mechanical Engineering, vol. 16, no. 4, pp. 7413–7429, 2019, doi: 10.15282/ijame.16.4.2019.15.0549

[11] R.K. Upadhyay, A. Kumar, *Epoxy-graphene-MoS2 composites with improved tribological behavior under dry sliding contact*, Tribiology International, vol. 130, pp. 106–118, 2019, doi: 10.1016/j.triboint.2018.09.016

[12] H. Singh, P. Singh, H. Bhowmick, *Influence of MoS2, H3BO3, and MWCNT Additives on the Dry and Lubricated Sliding Tribology of AMMC-Steel Contacts*, Journal of Tribology, vol. 140, iss. 4, pp. 1–11, 2018, doi: 10.1115/1.4038957

[13] H. Patle, P. Mahendiran, B.R. Sunil, R. Dumpala, *Hardness and sliding wear characteristics of AA7075-T6 surface composites reinforced with B4C and MoS2 particles*, Materials Research Express, vol. 6, no. 8, p. 086589, 2019, doi: 10.1088/2053-1591/ab1ff4

[14] N. Panwar, S. Saini, A. Chauhan, *Frictional study of Al 6061 red-mud composite under the influence of different process parameters*, Tribology in Industry, vol. 41, no. 2, pp. 199–211, 2019, doi: 10.24874/ti.2019.41.02.06

[15] G. Taguchi, *Introduction to quality engineering: designing quality into products and processes*, Tokyo: Asian Productivity Organization, 1986, p. 191, doi: 10.1002/qre.4680040216

[16] R.S.S. Raju, G.S. Rao, *Assessment of Tribological performance of Coconut Shell Ash Particle Reinforced Al-Si-Fe Composites using Grey-Fuzzy Approach*, Tribology in Industry, vol. 39, no. 3, pp. 364–377, 2017, doi: 10.24874/ti.2017.39.03.12

[17] Y. Sahin, *Tribological behaviour of metal matrix and its composite*, Materials & Design, vol. 28, iss. 4, pp. 1348–1352, 2007, doi: 10.1016/j.matdes.2006.01.032

[18] N. Miloradovic, B. Stojanovic, S. Mitrovic, S. Veličkovic, *Application of Taguchi method in the optimization of end milling parameters*, Proceedings on Engineering Sciences, vol. 1, no. 1, pp. 104–109, 2019, doi: 10.24874/PES01.01.014

[19] J.F. Lin, C.C. Chou, *The response surface method and the analysis of mild oxidational wear*, Tribology International, vol. 35, iss. 11, pp. 771–785, 2002, doi: 10.1016/S0301-679X(02)00030-0

[20] B.G. Park, A.G. Crosky, A.K. Hellier, *Fracture toughness of microsphere Al2O3-Al particulate metal matrix composites*, Composites Part B: Engineering, vol. 39, iss. 7–8, pp. 1270–1279, 2008, doi: 10.1016/j.compositesb.2008.01.005

[21] S. Das, S.V. Prasad, T.R. Ramachandran, *Microstructure and wear of cast (Al-Si alloy)-graphite composites*, Wear, vol. 133, iss. 1, pp. 173–187, 1989, doi: 10.1016/0043-1648(89)90122-1

[22] M.S. Phadke, *Quality Engineering Using Robust Design*, Prentice Hall, 1989.

[23] N. Raj, N. Radhika, *Tribological Characteristics of LM13/Si3N4/Gr Hybrid Composite at Elevated Temperature*, Silicon, vol. 11, iss. 2, pp. 947–960, 2019, doi: 10.1007/s12633-018-9893-1

[24] B. Chen, J. Zhang, Z. Liang, X. Yi, Z. Zhang, *Effects of MoS2 on tribological properties and mechanically mixed layer of al matrix composites*, Materials Science Forum, vol. 896, pp. 83–96, 2017, doi: 10.4028/www.scientific.net/MSF.896.83

[25] D. Dzunic, M. Pantic, S. Mitrovic, M. Babic, S. Petrovic Savic, A. Dordevic, A. Kokic Arsic, *Assessment Of Tribological Behaviour Of Za-27 Zinc-Aluminium Alloy Based Nanocomposite*, Proceedings on Engineering Sciences vol. 1, no. 1, pp. 145–153, 2019, doi: 10.24874/PES01.01.020